Fizika Nizkikh Temperatur, 2011, v. 37, No. 8, p. 860–866

X-ray magnetic circular dichroism in Co_2FeGa: First-principles calculations

D.A. Kukusta[1,2], V.N. Antonov[1,2], and A.N. Yaresko[1]

[1]*Max-Planck-Institut für Festkörperforschung, Heisenbergstrasse 1, D-70569 Stuttgart, Germany*

[2]*Institute for Metal Physics, 36 Vernadsky Str., 03142 Kiev, Ukraine*
E-mail: v.antonov@fkf.mpg.de

Received December 12, 2010

The electronic structure and x-ray magnetic circular dichroism (XMCD) spectra of the Heusler alloy Co_2FeGa were investigated theoretically from first principles, using the fully relativistic Dirac linear MT-orbital (LMTO) band structure method. Densities of valence states, orbital and spin magnetic moments are analyzed and discussed. The origin of the XMCD spectra in the Co_2FeGa compound is examined. The calculated results are compared with available experimental data.

PACS: 75.50.Cc Other ferromagnetic metals and alloys;
71.20.Lp Intermetallic compounds;
71.15.Rf Relativistic effects.

Keywords: strongly correlated systems, electronic structure, x-ray magnetic circular dichroism.

1. Introduction

Electronic devices exploiting the spin of an electron have being attracted great scientific interest [1]. Their basic element is a ferromagnetic electrode providing a spin-polarized electric current. In this context the most interesting materials are ones with a complete spin-polarization at the Fermi level. The rapid development of magneto-electronics intensified the interest in such materials. Addition of the spin degree of freedom to conventional electronic devices has several advantages such as the nonvolatility, the increased data processing speed, the decreased electric power consumption and the increased integration densities [1,2]. The current advances in new materials are promising for engineering new spintronic devices in the near future [2].

A metal for spin-up and a semiconductor for spin-down electrons is called half-metallic ferromagnet (HMF) [3], and Heusler compounds have been considered potential candidates to show this property. The full Heusler alloys are defined as well-ordered ternary intermetallic compounds, at the stoichiometric composition X_2YZ, which have the cubic $L2_1$ structure. These compounds involve two different transition metal atoms X, and Y, and a third element Z which is a nonmagnetic metal or nonmetallic element. Currently the Heusler alloys are at the focus of a large scientific interest due to their potential for applications in magnetic field sensors and spintronic devices [1]. In this paper we investigate the Heusler alloy Co_2FeGa. This compound is one of the most promising candidates for spintronic applications.

The magnetic structure of Co_2FeGa was studied by M. Kawakami *et al*. [4]. They measured the V and Mn hyperfine field in two types of diluted magnetic compounds, namely $Co_2T_{1-x}V_xGa$ and $Co_2T_{1-y}Mn_yGa$, where T = (Ti, Cr, Fe). The extrapolated local magnetic moments in Co_2FeGa were found to be $\mu_{Co} = (0.9 \pm 0.1)\mu_B$, $\mu_{Fe} = (3.4 \pm 0.3)\mu_B$ as $x \to 0$ and $\mu_{Co} = (1.0 \pm 0.1)\mu_B$, $\mu_{Fe} = (3.1 \pm 0.3)\mu_B$ as $y \to 0$. The total magnetic moment of Co_2FeGa was estimated to be equal to 5.19 μ_B/f.u.

The spin density in Co_2FeGa has been measured in a magnetic Compton scattering experiment [5]. The magnetic Compton profiles for the [100], [110], and [111] principal directions show anisotropy in the momentum density which is in good agreement with the results of full-potential linear augmented plane wave (FLAPW) calculations [5]. The theoretically calculated 3*d* spin moments at the Co and Fe sites have been found to be 1.20 μ_B and 2.66 μ_B. Authors analyzed the total and partial densities of states and revealed that Co_2FeGa can not be classified as a half metallic ferromagnet.

The magnetic and transport properties of the Co_2FeGa investigated by Ming Zhang *et al*. [6]. The lattice parameter was found to be $a = (5.727 \pm 0.012)$ Å. The spontaneous moment at 5 K obtained by extrapolation corresponds to

5.15 μ_B/f.u. The temperature dependence of the magnetization follows the spin-wave behavior at low temperature. The electrical resistivity behaves according to a $T^{2.1}$ power law, which may be mainly attributed to electron–electron scattering, and the contribution of electron–phonon scattering to the resistivity, which can give rise to T^5 behavior, seems to be small. At the temperatures 60 K $< T <$ 250 K, the electrical resistivity evolves to nearly linear $T^{1.31}$ power law. Point contact Andreev reflection measurements of the spin-polarization yield a polarization of 59%, which is in consistent with the theoretical prediction by a first-principles calculations [6]. The authors have shown that the loss of half-metalicity is due to strong hybridization between the Co $3d$ and Fe $3d$ states, resulting in a marked reduction of the spin polarization ratio P for the Co_2FeGa alloy.

Magnetic properties of $Co_2Cr_{1-x}Fe_xGa$ (x = 1.00, 0.80, 0.50, 0.25 and 0.0) Heusler alloys investigated by Umetsu *et al*. [7]. Room temperature lattice constants a for x = = 1.00 were equal to 5.741 Å. For x = 1.00, the value of saturation magnetization is about 5.17 μ_B/f.u., larger than the expected value of 5 μ_B/f.u. from the generalized Slater–Pauling line. The authors expect that such a large value of the magnetic moment would be explained by taking into account the contribution from the orbital magnetic moment. They found the value of Curie temperature T_C increases with increasing x and is about 1093 K for Co_2FeGa. The theoretical investigations have not revealed the half-metalicity in Co_2FeGa. Large ratios of the spin polarization P in $Co_2Cr_{1-x}Fe_xGa$ series have been obtained not only in the $L2_1$-type phase but also in the $B2$-type one. The half-metalicity becomes weaker with increasing x, because a large DOS for Cr at E_F in the majority spin band disappears and the gap in the minority spin band becomes narrow due to the hybridization between Fe $3d$ and Co $3d$ states. For Co_2FeGa they have found the spin polarization ratio to be slightly larger than 40%.

The Curie temperature for the Heusler compound Co_2FeGa was theoretically estimated in a frame of the local-density approximation in Ref. 8. The theoretically calculated value T_C^{theory} = 1185 K was found to be in a good agreement with the experimental measurements T_C^{exp} = 1100 K.

The ternary nanoparticles based on the Heusler compound Co_2FeGa have been prepared and investigated by means of x-ray diffraction (XRD), transmission electron microscopy, temperature dependent magnetometry and Mössbauer spectroscopy by L. Basit *et al*. [9]. All methods clearly revealed the Heusler-type $L2_1$ structure of the nanoparticles. In particular, anomalous XRD data demonstrate the correct composition in addition to the occurrence of the $L2_1$ structure. Mössbauer spectroscopy also has confirmed the Heusler-type character of the Co_2FeGa nanoparticles, with the obtained hyperfine magnetic field H_{hf} = 24.15 kA/m being in well agreement with the value obtained for bulk samples of Co_2FeGa. Namely, the Heusler-type character of the particles has been revealed by the absence of a quadrupole splitting of the spectrum unambiguously indicating the cubic environment of the iron atoms and confirming the O_h symmetry of the Fe sites expected in the Heusler-type $L2_1$ structure. The lattice parameter has been determined to be a = (0.57310 ± 0.00008) nm at room temperature (300 K). This value is about 0.24% smaller than in polycrystalline bulk material. The magnetic moment of the particles is about 5 μ_B at low temperature in good agreement with the value of bulk material. This suggests that the magnetic properties are conserved even in particles on the 10–15 nm scale.

This paper is devoted to the theoretical calculations of the electronic structure and x-ray magnetic circular dichroism in Co_2FeGa. Recently x-ray magnetic circular dichroism measurements in the ferromagnetic Co_2FeGa were carried out by Umetsu *et al*. [10] at the Co, Fe and Ga $L_{2,3}$ edges.

This paper is organized as follows. Section 2 presents a description of Co_2FeGa crystal structure as well as the computational details. Section 3 is devoted to the electronic structure and XMCD spectra of $CeFe_2$ calculated with the fully relativistic Dirac LMTO band structure method. The calculated results are compared with the available experimental data. Finally, the results are summarized in Sec. 4.

2. Crystal structure and computational details

The Heusler-type X_2YZ compound crystallizes in the cubic $L2_1$ structure with $Fm\bar{3}m$ space group (No. 225). It is formed by four interpenetrating fcc sublattices as shown in Fig. 1. The X ions occupy the $8c$ Wyckoff positions (x = 1/4, y = 1/4, z = 1/4). The Y ions occupy the $4a$ positions (x = 0, y = 0, z = 0), and the Z ions are placed at the $4b$ sites (x = 1/2, y = 1/2, z = 1/2). All atoms have eight nearest neighbors at the same distance. The Y and Z atoms have eight X atoms as nearest neighbors, while for X there are four Y and four Z atoms.

The details of the computational method are described in the previous papers [11,13], and here we only mention

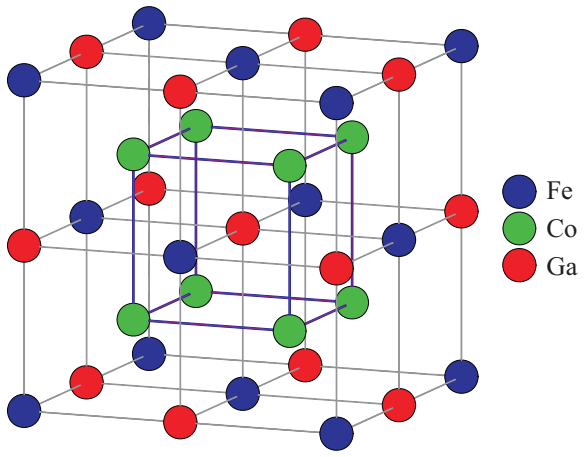

Fig. 1. (Color online) Schematic representation of the $L2_1$ structure. The cubic cell contains four primitive cells.

some aspects specific to the present calculations. The calculations were performed using the spin-polarized fully relativistic linear-muffin-tin-orbital (SPR LMTO) method [14,15] with the combined correction term taken into account. The LSDA part of the calculations was based on the spin-density functional with the Perdew–Wang [16] of the exchange-correlation potential. Brillouin zone (BZ) integrations were performed using the improved tetrahedron method [17] and charge self-consistency was obtained on a grid of 331 **k** points in the irreducible part of the BZ. The basis consisted of *s*, *p*, *d*, and *f* LMTO's.

The intrinsic broadening mechanisms have been accounted for by folding the XMCD spectra with a Lorentzian. For the finite lifetime of the core hole a constant width Γ_c, in general from Ref. 18, has been used. The finite apparative resolution of the spectrometer has been accounted for by a Gaussian of 0.9 eV

3. Results and discussion

3.1. Energy band structure

The total and partial DOS's of Co_2FeGa are presented in Fig. 2. The results agree well with previous band structure calculations [5,7,8]. The occupied part of the valence band can be subdivided into several regions. Ga 2*s* states appear between -10.5 eV and -7.0 eV. The states in the energy range -5.5 eV to 4.0 eV are formed by Co and Fe *d* states and Ga *p* states. Co_2FeGa has a local magnetic moments of $M_S = 1.103\mu_B$, $M_l = 0.048\mu_B$ on Co, $M_S = 2.694\mu_B$, $M_l = 0.069\mu_B$ on Fe, and $M_S = -0.065\mu_B$ (see Table 1). The total magnetic moment was found to be equal to 4.83 μ_B.

Table 1. The experiment and calculated spin M_s, orbital M_l, and total $M_s + M_l$ magnetic moments (in μ_B) of Co_2FeGa

Method	Atom	M_s	M_l	M_s+M_l	Total M_s
LSDA	Co	1.103	0.048	1.151	4.83
	Fe	2.694	0.069	2.763	
Sum rules	Co	0.681	0.027	0.708	3.25
	Fe	1.775	0.040	1.815	
Sum rules[a]	Co	1.071	0.049	1.120	4.79
	Fe	2.496	0.068	2.564	
Sum rules[b]	Co	1.089	0.050	1.139	4.86
	Fe	2.525	0.069	2.594	
Exper. [10] (sum rules)	Co	1.22	0.08	1.30	5.4
	Fe	2.96	0.06	3.02	
Exper. [10] (hyperfine field)	Co	–	–	0.9±0.1	5.2
	Fe	–	–	3.4±0.1	

[a]Sum rules applied for the XMCD spectra calculated ignoring the energy dependence of the radial matrix elements.

[b]Sum rules applied for the XMCD spectra calculated ignoring the energy dependence of the radial matrix elements and ignoring $p \to s$ transitions.

The hybridization between Fe and Co *d* states plays an important role in the formation of the band structure of Co_2FeGa. It leads to the splitting of the *d* states into the bonding states which have Co and Fe *d* character and antibonding states at about 1 eV above E_F with stronger contribution of Fe *d* states. We should mention that the spin-orbital splitting of *d* states on $d_{3/2}$ and $d_{5/2}$ is much smaller than the splitting caused by the crystal field. At the Co 8*c* site (T_d point symmetry) it causes the splitting of *d* orbitals into a doublet *e* ($3z^2 - 1$ and $x^2 - y^2$) and a triplet t_2 (*xy*, *yz*, and *xz*). The crystal field at the Fe 4*a* site (O_h point symmetry) splits Fe *d* states into e_g ($3z^2 - 1$ and $x^2 - y^2$) and t_{2g} (*xy*, *yz*, and *xz*) states.

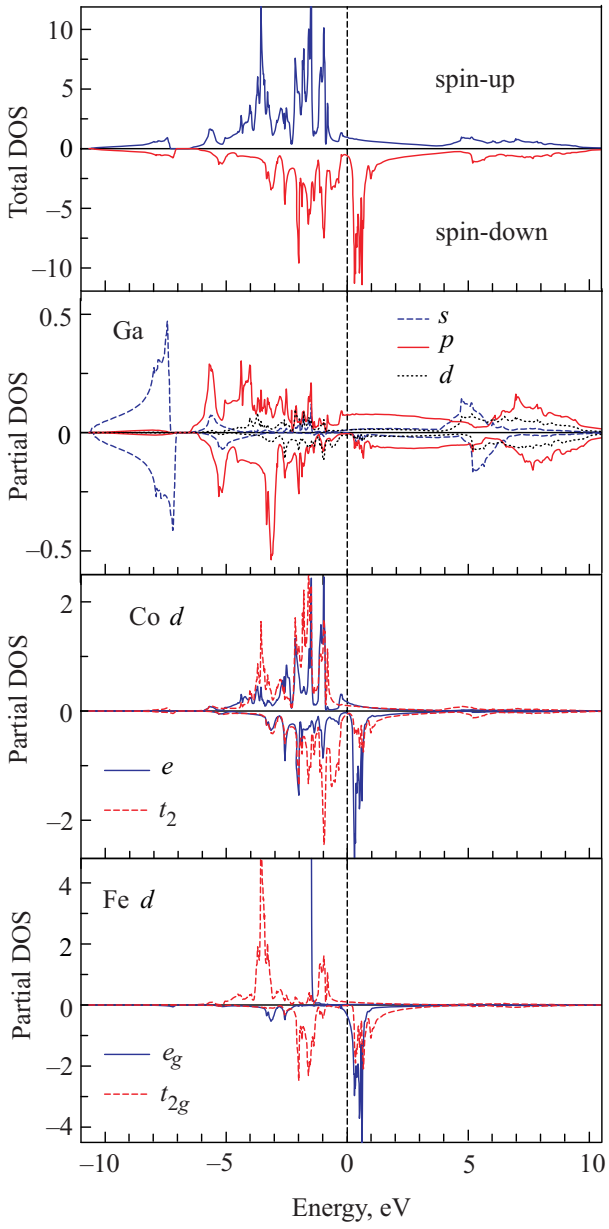

Fig. 2. (Color online) The total (in states/(cell·eV)) and partial (in states/(atom·eV)) density of states of Co_2FeGa. The Fermi energy is at zero.

3.2. XMCD spectra

At the core level edge XMCD is not only element-specific but also orbital specific. For 3*d* transition metals, the electronic states can be probed by the *K*, $L_{2,3}$ and $M_{2,3}$ x-ray absorption and emission spectra. The experimental measurements of the XMCD spectra in ferromagnetic Co_2FeGa were carried out by Umetsu *et al*. [10] at the Co, Fe and Ga $L_{2,3}$ edges. Authors estimated the ratios of the orbital magnetic moment to the spin magnetic moment M_{orb}/M_{spin} being equal to 0.06 and 0.02 for Co and Fe, respectively. The application of the sum rules leads to $M_S = 1.22\mu_B$, $M_l = 0.08\mu_B$ per Co atom and $M_S = 2.96\mu_B$, $M_l = 0.06\mu_B$ per Fe atom. The orbital magnetic moments of these two elements were found to be small. The contribution from the Ga magnetic moment which might be induced in the conduction band to the total magnetic moment is considered to be negligibly small, though a small finite moment in the Ga 4*s* states was found.

Figure 3 shows the XAS and XMCD spectra at the Co $L_{2,3}$ edges calculated in the LSDA approach together with the experimental data [10]. The corresponding spectra for Fe and Ga are presented in Figs. 4 and 5, respectively.

Because of the dipole selection rules, apart from the $4s_{1/2}$ states (which have a small contribution to the XAS due to relatively small $2p \to 4s$ matrix elements) only $3d_{3/2}$ states occur as final states for L_2 XAS for unpolarized radiation, whereas for the L_3 XAS the $3d_{5/2}$ states also contribute [19]. Although the $2p_{3/2} \to 3d_{3/2}$ radial matrix elements are only slightly smaller than for the $2p_{3/2} \to 3d_{5/2}$ transitions the angular matrix elements strongly suppress the $2p_{3/2} \to 3d_{3/2}$ contribution [19]. Therefore neglecting the energy dependence of the radial matrix elements, the L_2 and the L_3 spectrum can be viewed as a direct mapping of the DOS curve for $3d_{3/2}$ and $3d_{5/2}$ character, respectively.

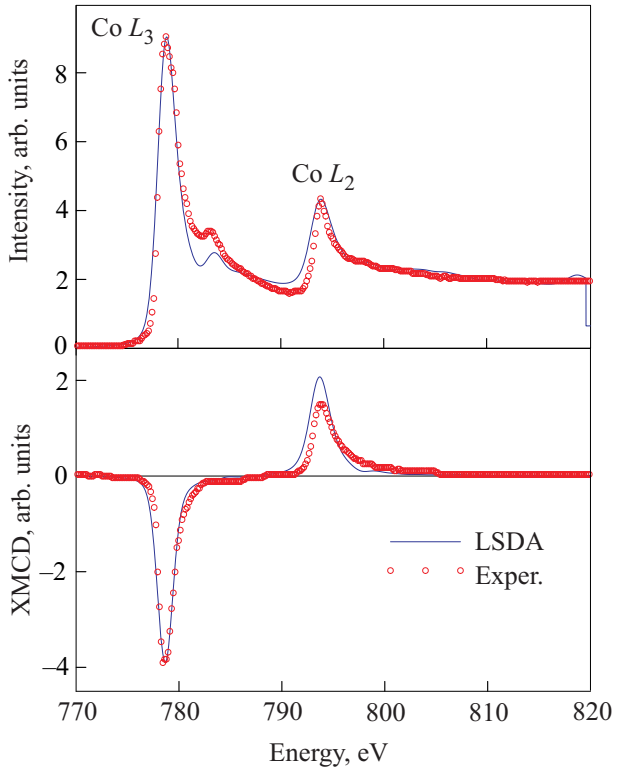

Fig. 3. (Color online) Upper panel: calculated as well as experimental (circles) x-ray absorption spectra of Co_2FeGa at the Co $L_{2,3}$ edges. Experimental spectra [10] were measured by means of total photoelectron yield with external magnetic field 1.9 T at 18 K. Low panel: theoretically calculated in LDSA and experimental [10] (circles) XMCD spectra of Co_2FeGa at the Co $L_{2,3}$ edges.

The experimental Co XAS has a pronounced shoulder at the L_3 peak at around 783 eV shifted by about 4 eV with respect to the maximum to higher photon energy. This structure is less pronounced at the L_2 edge, which can be ascribed to the lifetime broadening effect because the lifetime of the $2p_{1/2}$ core hole is shorter than the $2p_{3/2}$ core hole due to the L_2L_3V Coster–Kronig decay. This feature is partly due to the interband transitions from $2p$ core level to Co 3*d* empty states at around 5 eV above the Fermi level. Actually, as can be seen from Fig. 2, Co d partial DOS's have two pronounced peaks at 0.5 eV and approximately 5 eV above the Fermi level. Both the features are reflected in the theoretically calculated XAS at the Co L_3 edge around 779 and 783 eV, respectively (Fig. 3), although the second peak is less pronounced in the theoretical spectrum.

Figure 4 presents the calculated XAS as well as XMCD spectra of the Co_2FeGa compound at the Fe $L_{2,3}$ edges together with the experimental data [10]. The peak in the empty partial Fe d DOS at around 7 eV above the Fermi level is less intensive in comparison with the corresponding peak in the Co d partial DOS (see Fig. 2), therefore the high-energy fine structure is less pronounced and shifted towards higher energy in comparison with the similar structure in the Fe XAS (compare Figs. 3 and 4).

It may be seen in the upper panel of Fig. 3 that the experimentally measured Co L_3 XAS has some additional intensity around 783 eV above E_F which is not completely reproduced by the theoretical calculations. A similar situation also appear in the Fe L_3 XAS (Fig. 4) where the theoretical one-particle calculations does not reproduce all the intensity at around 712 eV. This might indicate that additional satellite structures may appear due to many-body effects at the high-energy tails of both the Co and Fe $L_{2,3}$ XAS's. This question needs additional theoretical investigation using an appropriate many-body treatment.

The calculated Co and Fe $L_{2,3}$ XMCD spectra are in good agreement with the experiment [10], although the calculated magnetic dichroism is somewhat too high at the L_2 edge. One of the reasons for this discrepancy might be the core-hole effect [20]. When the 2*p* core electron is photo-excited to the unoccupied d states, the distribution of the charge changes to account for the created hole. We have taken into account this effect in the additional electronic structure calculations using super-cell approximation

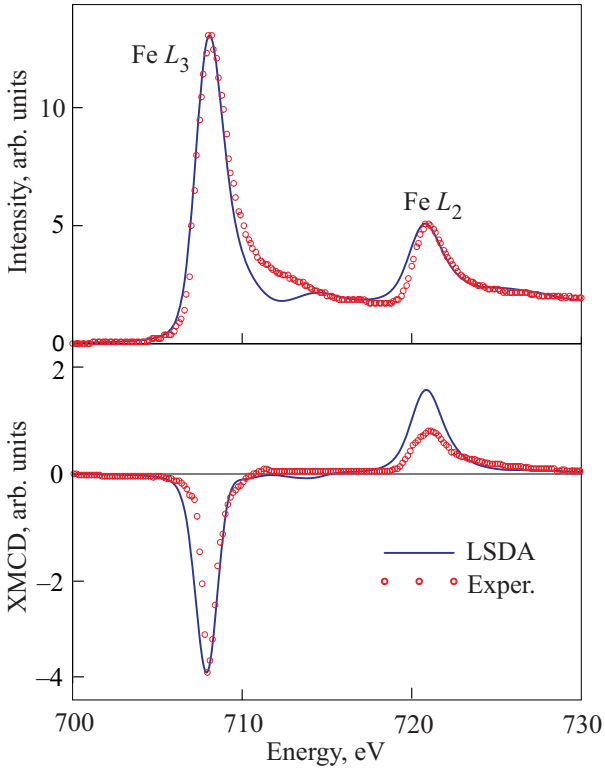

Fig. 4. (Color online) Upper panel: calculated as well as experimental (circles) x-ray absorption spectra of Co_2FeGa at the Fe $L_{2,3}$ edges. Experimental spectra [10] were measured by means of total photoelectron yield with external magnetic field 1.9 T at 18 K. Low panel: theoretically calculated in LDSA and experimental [10] (circles) XMCD spectra of Co_2FeGa at the Fe $L_{2,3}$ edges.

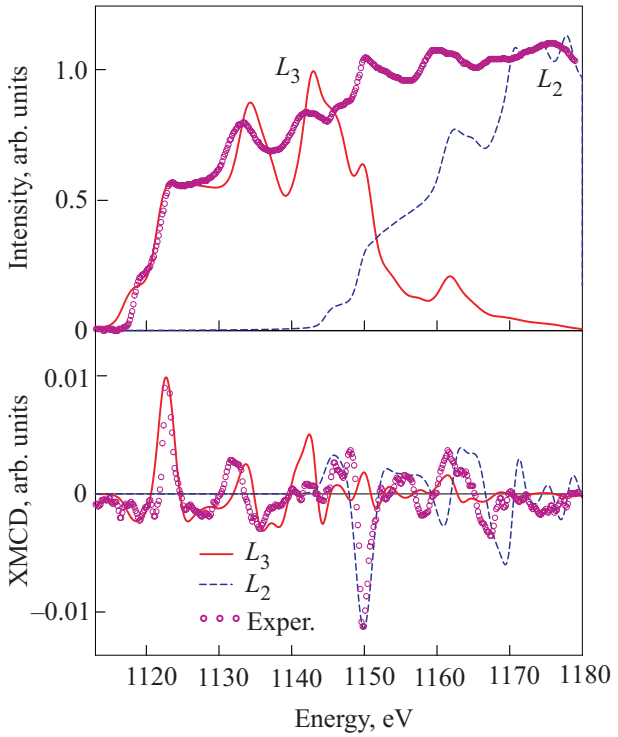

Fig. 5. (Color online) Upper panel: calculated as well as experimental (circles) x-ray absorption spectra of Co_2FeGa at the Ga $L_{2,3}$ edges. Experimental spectra [10] were measured by means of total photoelectron yield with external magnetic field 1.9 T at 18 K. Low panel: theoretically calculated in LDSA and experimental [10] (circles) XMCD spectra of Co_2FeGa at the Ga $L_{2,3}$ edges.

and found that the agreement with the experimental XMCD spectra is slightly improved (not shown) so such the effect does not fully explain the overestimation of the XMCD at the L_2 edge. This question also needs additional theoretical investigation.

Figure 5 presents the calculated XAS as well as XMCD spectra of the Co_2FeGa compound at the Ga $L_{2,3}$ edges compared with the experimental data [10]. The Ga partial d DOSs are extended from -5 eV to more than 10 eV above Fermi level E_F. Therefore the Ga L_2 and L_3 x-ray absorption spectra are wide-ranged and strongly overlaped (see Fig. 5). The Ga $L_{2,3}$ XA spectra have four major peaks located at the 1123, 1134, 1142, 1152, 1161 eV and flat structure at around 1172 to 1180 eV range. The low-energy peak at the 1123 eV also has well defined shoulder at 1119 eV. The first three low-energy peaks belong to the L_3 XAS, the high-energy peak at the 1161 eV and flat structure at around 1172 to 1180 eV are mostly determined by the x-ray absorption at the L_2 edge. However, both the L_3 and L_2 equally contribute to the intensity of the peak at the 1152 eV. The energy position of the L_3 low-energy peaks at the 1123 eV and L_2 peaks at the 1161 and 1175 eV are well reproduced by the theory. However, the theoretically calculated peaks at the 1134 and 1142 eV are shifted towards higher energies. One of possible reason for such the discrepancy is linearized nature of the LMTO band structure method [14].

The XMCD spectra have major peaks at the 1122 and 1150 eV at the L_3 and L_3 edges, respectively, with opposite signs and additional fine structures at higher energies. The theory quite well describe the intensity and energy position of these major peaks, however, the energy position of higher energy peaks are shifted in comparison with the experimental measurements as it was observed in the x-ray absorption. Besides, for the energies higher than peak at 1132 eV for the L_3 spectrum and above 1167 eV for the L_3 spectrum theory gives some additional oscillating structures, while the experimental spectrum is a smooth function of energy. Such the oscillation behavior of the high-energy part of the theoretical spectra could possibly be damped by the quasiparticle life-time effect, which is not taken into account in our calculations.

3.3. Magnetic moments

In magnets, the atomic spin M_S and orbital M_l magnetic moments are basic quantities and their separate determination is therefore important. The methods of their experimental determination include traditional gyromagnetic ratio measurements [21], magnetic form factor measure-

ments using neutron scattering [22], and magnetic x-ray scattering [23]. In addition to these, the recently developed x-ray magnetic circular dichroism combined with several sum rules [24–27] has attracted much attention as a method of site- and symmetry-selective determination of M_S and M_l.

Because of the significant implications of the sum rules, numerous experimental and theoretical studies aimed at investigating their validity for itinerant magnetic systems have been reported, but with widely different conclusions. The claimed adequacy of the sum rules varies from very good (within 5% agreement) to very poor (up to 50% discrepancy) [19]. This lack of a consensus may have several origins. On the theoretical side, it has been demonstrated by circularly polarized 2*p* resonant photoemission measurements of Ni that both the band structure effects and electron–electron correlations are needed to satisfactorily account for the observed XMCD spectra [28]. However, it is extremely difficult to include both of them in a single theoretical framework. Besides, the XAS as well as XMCD spectra can be strongly affected (especially for the early transition metals) by the interaction of the excited electron with the created core hole [20,29]. On the experimental side, the indirect x-ray absorption techniques, i.e., the total electron and fluorescence yield methods, are known to suffer from saturation and self-absorption effects that are very difficult to correct for Ref. 30. They are sensitive to the varying applied magnetic field, changing the electron detecting efficiency, or, equivalently, the sample photocurrent [31].

The Fe L_3 and L_2 spectra in Co_2FeGa are strongly overlapped therefore the decomposition of a corresponding experimental $L_{2,3}$ spectrum into its L_3 and L_2 parts is quite difficult and can lead to a significant error in the estimation of the magnetic moments using the sum rules since the integration $\int_{L_3}$ and $\int_{L_2}$ must be taken over the $2p_{3/2}$ and $2p_{1/2}$ absorption regions separately. Besides, the experimentally measured Co and Fe $L_{2,3}$ x-ray absorption spectra have background scattering intensity and the integration of the corresponding XASs may lead to an additional error in the estimation of the magnetic moments using the sum rules.

We have compared the spin and orbital moments obtained from the theoretically calculated XAS and XMCD spectra through sum rules with directly calculated LSDA values in order to avoid additional experimental problems. The number of the transition metal 3*d* electrons is calculated by integrating the occupied *d* partial density of states inside the corresponding atomic sphere which gives the values averaged for the nonequivalent sites $n_{Co} = 2.27$ and $n_{Fe} = 3.48$. Sum rules reproduce the LSDA spin magnetic moments within 38%, and 34% and the orbital moments within 44 and 42% for Co and Fe, respectively (Table 1). It is well known that the XMCD sum rules have been derived within an ionic model using a number of approximations. For $L_{2,3}$, they are [32]: (1) ignoring the exchange splitting of the core levels; (2) replacing the interaction operator $\boldsymbol{\alpha} \cdot \mathbf{a}_\lambda$ by $\nabla \cdot \mathbf{a}_\lambda$; (3) ignoring the asphericity of the core states; (4) ignoring the difference of $d_{3/2}$ and $d_{5/2}$ radial wave functions; (5) ignoring $p \to s$ transitions; (6) ignoring the energy dependence of the radial matrix elements. To investigate the influence of the last point we applied the sum rules to the Co, and Fe XMCD spectra neglecting the energy dependence of the radial matrix elements. As can be seen from Table 1 using the energy independent radial matrix elements reduces the disagreement in spin magnetic moments to 2.9 and 7.3% and in the orbital moment to 2.1 and 1.4% for Co and Fe, respectively. Additionally the omitting of the $p \to s$ transitions leads to mainly the same results as in the previous case but the mentioned above disagreement is decreased (being within 2.4 and 6.2% for the spin moments at the Co and Fe sites, respectively, as well as 4.2% and less than 1% for the orbital moments for both sites). These results show that the energy dependence of the matrix elements and the presence of $p \to s$ transitions affect strongly the values of both the spin and the orbital magnetic moments derived from the sum rules.

4. Summary

We have studied the electronic structure and x-ray magnetic circular dichroism spectra of the Heusler alloy Co_2FeGa by means of an *ab initio* fully-relativistic spin-polarized Dirac linear muffin-tin orbital method.

The spin-polarized LSDA calculations show that Co_2FeGa is a ferromagnet. The band structure calculations in the LSDA approximation well reproduce the shape of the XAS and XMCD spectra at the Co and Fe $L_{2,3}$ edges. The shape of the Ga XAS and XMCD is reproduced in less accurate way due to extended behavior of Ga partial *d*-DOSs.

XMCD sum rules are derived within an ionic model using a number of approximations. The most important are the energy dependence of the matrix elements and the presence of $s \to p$ transitions omitted in the sum rules. The adequacy of sum rules varies from 10 to 100% depending of the degree of localization of the valence states.

Acknowledgments

D.A. Kukusta and V.N. Antonov gratefully acknowledge the hospitality at Max-Planck-Institut für Festkörperforschung in Stuttgart during their stay.

1. G.A. Prinz, *Science* **282**, 1660 (1998).
2. S.A. Wolf, D.D. Awschalom, R.A. Buhrman, J.M. Daughton, S. von Molnar, M.L. Roukes, A.Y. Chtchelkanova, and D.M. Treger, *Science* **294**, 1488 (2001).
3. R.A. de Groot, F.M. Mueller, P.G. van Engen, and K.H.J. Buschow, *Phys. Rev. Lett.* **50**, 2024 (1983).
4. M. Kawakami, M. Nagahama, and S. ichi Satohira, *J. Phys. Soc. Jpn.* **59**, 4466 (1990).

5. A. Deb, M. Itou, Y. Sakurai, N. Hiraoka, and N. Sakai, *Phys. Rev*. **B63**, 064409 (2001).
6. M. Zhang, E. Brück, F.R. de Boer, Z. Li, and G. Wu, *J. Phys*. **D37**, 2049 (2004).
7. R.Y. Umetsu, K. Kobayashi, A. Fujita, K. Oikawa, R. Kainuma, K. Ishida, N. Endo, K. Fukamichi, and A. Sakuma, *Phys. Rev*. **B72**, 214412 (2005).
8. J. Kübler, G.H. Fecher, and C. Felser, *Phys. Rev*. **B7**6, 024414 (2007).
9. L. Basit, C. Wang, C.A. Jenkins, B. Balke, V. Ksenofontov, G.H. Fecher, C. Felser, E. Mugnaioli, U. Kolb, S.A. Nepijko, G. Schonhense, and M. Klimenkov, *J. Phys*. **D42**, 084018 (2009).
10. R.Y. Umetsu, T. Nakamura, K. Kobayashi, R. Kainuma, A. Sakuma, K. Fukamichi, and K. Ishida, *J. Phys*. **D43**, 105001 (2010).
11. V.N. Antonov, H.A. Dürr, Y. Kucherenko, L.V. Bekenov, and A.N. Yaresko, *Phys. Rev*. **B72**, 054441 (2005).
12. V.N. Antonov, A.P. Shpak, and A.N. Yaresko, *Fiz. Nizk. Temp*. **34**, 3 (2008) [*Low Temp. Phys*. **34**, 1 (2008)].
13. V. Antonov, D. Kukusta, A. Shpak, and A. Yaresko, *Condens. Matter Phys*. **11**, 627 (2008).
14. O.K. Andersen, *Phys. Rev*. **B12**, 3060 (1975).
15. V.V. Nemoshkalenko, A.E. Krasovskii, V.N. Antonov, V.N. Antonov, U. Fleck, H. Wonn, and P. Ziesche, *Phys. Status Solidi* **B120**, 283 (1983).
16. J. Perdew and Y. Wang, *Phys. Rev*. **B45**, 13244 (1992).
17. P.E. Blöchl, O. Jepsen, and O.K. Andersen, *Phys. Rev*. **B49**, 16223 (1994).
18. J.C. Fuggle and J.E. Inglesfield, *Unoccupied Electronic States. Topics in Applied Physics*, vol. 69, Springer, New York (1992).
19. V. Antonov, B. Harmon, and A. Yaresko, *Electronic Structure and Magneto-Optical Properties of Solids*, Kluwer, Dordrecht (2004).
20. J. Schwitalla and H. Ebert, *Phys. Rev. Lett*. **80**, 4586 (1998).
21. G.G. Scott, *J. Phys. Soc. Jpn*. **17**, 372 (1962).
22. W. Marshall and S.W. Lovsey, *Theory of Thermal Neutron Scattering*, Oxford University Press, Oxford (1971).
23. M. Blume, *J. Appl. Phys*. **57**, 3615 (1985).
24. G. van der Laan and B.T. Thole, *Phys. Rev*. **B38**, 3158 (1988).
25. B.T. Thole, P. Carra, F. Sette, and G. van der Laan, *Phys. Rev. Lett*. **68**, 1943 (1992).
26. P. Carra, B.T. Thole, M. Altarelli, and X. Wang, *Phys. Rev. Lett*. **70**, 694 (1993).
27. G. van der Laan and B.T. Thole, *Phys. Rev*. **B53**, 14458 (1996).
28. L.H. Tjeng, C.T. Chen, P. Rudolf, G. Meigs, G. van der Laan, and B.T. Thole, *Phys. Rev*. **B48**, 13378 (1994).
29. J. Zaanen, G.A. Sawatzky, J. Fink, W. Speier, and J.C. Fuggle, *Phys. Rev*. **B37**, 4905 (1985).
30. T. Böske, W. Clemens, C. Carbone, and W. Eberhardt, *Phys. Rev*. **B49**, 4003 (1994).
31. C.T. Chen, Y.U. Idzerda, H.-J. Lin, N.V. Smith, G. Meigs, E. Chaban, G.H. Ho, E. Pellegrin, and F. Sette, *Phys. Rev. Lett*. **75**, 152 (1995).
32. H. Ebert, *Rep. Prog. Phys*. **59**, 1665 (1996).